PHYSICAL REVIEW D **96,** 034509 (2017)

# Evidence of effective axial $U(1)$ symmetry restoration at high temperature QCD

A. Tomiya,[1] G. Cossu,[2] S. Aoki,[3] H. Fukaya,[4] S. Hashimoto,[5,6] T. Kaneko,[5,6] and J. Noaki[5]

(JLQCD Collaboration)

[1]*Key Laboratory of Quark & Lepton Physics (MOE) and Institute of Particle Physics, Central China Normal University, Wuhan 430079, China*
[2]*School of Physics and Astronomy, The University of Edinburgh, Edinburgh EH9 3JZ, United Kingdom*
[3]*Center for Gravitational Physics, Yukawa Institute for Theoretical Physics, Kyoto University, Kyoto 606-8502, Japan*
[4]*Department of Physics, Graduate School of Science, Osaka University, Toyonaka 560-0043, Japan*
[5]*High Energy Accelerator Research Organization (KEK), Tsukuba 305-0801, Japan*
[6]*School of High Energy Accelerator Science, The Graduate University for Advanced Studies (Sokendai), Tsukuba 305-0801, Japan*

(Received 27 January 2017; published 10 August 2017; corrected 17 October 2017)

We study the axial $U(1)$ symmetry at a finite temperature in two-flavor lattice QCD. Employing the Möbius domain-wall fermions, we generate gauge configurations slightly above the critical temperature $T_c$ with different lattice sizes $L = 2$–$4$ fm. Our action allows frequent topology tunneling while keeping good chiral symmetry close enough to that of overlap fermions. This allows us to recover full chiral symmetry by an overlap/domain-wall reweighting. Above the phase transition, a strong suppression of the low-lying modes is observed in both overlap and domain-wall Dirac spectra. We, however, find a sizable violation of the Ginsparg-Wilson relation in the Möbius domain-wall Dirac eigenmodes, which dominates the signals of the axial $U(1)$ symmetry breaking near the chiral limit. We also find that the use of the overlap fermion only in the valence sector is dangerous since it suffers from the artifacts due to partial quenching. Reweighting the Möbius domain-wall fermion determinant to that of the overlap fermion, we observe the axial U(1) breaking to vanish in the chiral limit, which is stable against the changes of the lattice volume and lattice spacing.

DOI: 10.1103/PhysRevD.96.034509

## I. INTRODUCTION

The action of quantum chromodynamics (QCD) with two massless quark flavors has a global $SU(2)_L \times SU(2)_R \times U(1)_V \times U(1)_A$ symmetry. The flavor (or isospin) nonsinglet part $SU(2)_L \times SU(2)_R$ is spontaneously broken to the vectorlike subgroup $SU(2)_V$ below the critical temperature $T_c$ by the presence of the chiral condensate $\langle\bar{\psi}\psi\rangle \neq 0$. The axial $U(1)_A$ symmetry is, on the other hand, violated by anomaly. Namely, the flavor-singlet axial current is not conserved due to the topological charge density operator appearing in the axial Ward-Takahashi identity. Since this anomalous Ward-Takahashi identity is valid in any environment, the $U(1)_A$ symmetry is supposed to be violated at any temperature. Taking account of the gluonic dynamics, on the other hand, how much the topological charge density contributes to the low-energy physics may depend on the amount of topological activity in the background gauge field. In fact, at a high temperature $T \gg T_c$ [1], the instanton density is exponentially suppressed, and the $U(1)_A$ symmetry, as probed by physical observables, would be restored.

Just above the transition temperature $T_c$, topological fluctuations are not well understood theoretically, due to nonperturbative nature of QCD dynamics, and the question remains open about whether the $U(1)_A$ symmetry is effectively restored or not. It is related to the important question on the order and the critical exponents of the two-flavor QCD chiral phase transition, since the symmetry determines the properties of the transition as discussed in [2,3]. The fate of the $U(1)_A$ symmetry is also of phenomenological interest, since the topological susceptibility in the hot early Universe gives a strong constraint on the axion dark matter scenario [18–22].

One of the possible observables for the $U(1)_A$ symmetry breaking is the difference of flavor nonsinglet meson susceptibilities,

$$\Delta_{\pi-\delta} = \int d^4x[\langle\pi^a(x)\pi^a(0)\rangle - \langle\delta^a(x)\delta^a(0)\rangle], \quad (1)$$

where $\pi^a = \bar{\psi}\tau^a\gamma_5\psi$ and $\delta^a = \bar{\psi}\tau^a\psi$ represent the isospin triplet pseudoscalar and scalar operators, respectively. Here, $\tau^a$ denotes one of the $SU(2)$ generators. The measurement of (1) is relatively easy as it does not involve disconnected diagrams. Decomposing the quark propagator into the eigenmodes of the Dirac operator, $\Delta_{\pi-\delta}$ may be

 

written only in terms of its eigenvalue spectrum $\rho(\lambda)$ (in the continuum limit),

$$\Delta_{\pi-\delta} = \int_0^\infty d\lambda \rho(\lambda) \frac{2m^2}{(\lambda^2+m^2)^2}. \quad (2)$$

Here, the Dirac operator eigenvalue density is defined by $\rho(\lambda) = (1/V)\langle\sum_{\lambda'}\delta(\lambda-\lambda')\rangle$, with the four-dimensional volume $V = L^3 \times L_t$. To be precise, this relation is valid only in the large volume limit $L^3 \to \infty$. We need to take the spatial lattice size $L$ much larger than the correlation length of the system so that corrections of order $1/L$ are negligible. The size $L_t$ in the temporal direction corresponds to the inverse temperature $1/T$. Since the integrand of (2) at finite eigenvalue $\lambda$ vanishes in the massless limit, $\rho(0)$ (including its derivatives) controls whether $\Delta_{\pi-\delta}$ survives or not above the chiral phase transition temperature [23–25]. In fact, under an assumption of analyticity (in $m^2$), it can be shown that $\rho(0)$ vanishes *before* taking the massless limit [26], and therefore the integral (2) vanishes. Our previous work using overlap fermions [27], as well as the work by TWQCD Collaboration [28], supports this argument. We also note that a recent numerical simulation with Wilson fermions [29] and an analytic study [30] report that the $U(1)_A$ anomaly effect is consistent with zero in the chiral limit.

A possible counter argument to [26] is that the spectral function could be nonanalytic near $\lambda = 0$ in the infinite volume limit. Some of the recent lattice calculations suggest this possibility by finding a peak of $\rho(\lambda)$ near $\lambda = 0$ [31–33]. There is however a delicate issue due to the violation of chiral symmetry on the lattice, since the zero modes are necessarily chiral (left- or right-handed) in the continuum QCD, and even tiny violation of chiral symmetry in the lattice fermion formulation may induce spurious zero modes or destroy the physical zero modes. In fact, we demonstrated in [34] that the near-zero modes are largely affected by the violation of the Ginsparg-Wilson relation [35,36] even if one uses the Möbius domain-wall fermion, which suppresses the violation of chiral symmetry at the level of the residual mass being $O(1\text{ MeV})$.

In this work, we study the spectral function of the Dirac operator at a finite temperature in order to elucidate the possible effect of the residual chiral symmetry violation in the Möbius domain-wall fermion formulation. We introduce the reweighting technique to realize the formulation that exactly satisfies the Ginsparg-Wilson relation based on the ensembles generated with the Möbius domain-wall fermions [37,38]. Any difference between the spectral functions before and after the reweighting may indicate contamination due to imprecise chiral symmetry. In our previous work [27], we employed the overlap fermion formulation [39,40] that has exact chiral symmetry [41], but the simulation was restricted to a fixed topological sector [42,43]. We avoided this problem in the present work by generating ensembles with the Möbius domain-wall fermion that allows frequent topology changes during simulations.

We generate ensembles of two-flavor QCD configurations at temperatures in the range between 170 and 220 MeV that cover the temperature region slightly above the chiral phase transition. We employ the Möbius domain-wall fermion for the sea quark formulation to achieve good chiral symmetry, while allowing the topology tunnelings. Spatial volume sizes are in the range $L = 2$–$4$ fm. Degenerate bare quark masses are taken in the range 2–25 MeV.

As we will see below, we find a strong suppression of low-lying Dirac eigenvalues and the results for the Möbius domain-wall and overlap fermions agree with each other. The $U(1)_A$ susceptibility $\Delta_{\pi-\delta}$ is more subtle. It turns out that the violation of the Ginsparg-Wilson relation for the lowest modes of Möbius domain-wall fermion is much larger than what we expect from the residual mass $\sim O(1)$ MeV, and the violation dominates the signals of $\Delta_{\pi-\delta}$ [34]. We also find that the use of the overlap fermion only in the valence sector (as proposed in [33,44]) suffers from partially quenching artifacts. Replacing the Möbius domain-wall Dirac operator by the overlap Dirac operator both in valence and sea quarks, we find a strong suppression of $\Delta_{\pi-\delta}$ towards the chiral limit. The chiral extrapolation of $\Delta_{\pi-\delta}$ is consistent with zero, which is insensitive to the change of lattice volume $V$ and lattice spacing $a$.

The rest of this paper is organized as follows. In Sec. II, we explain the technical details of our numerical setup. The result for the Dirac eigenvalue spectrum is presented in Sec. III and that for the $U(1)_A$ susceptibility is given in Sec. IV. Our conclusions are given in Sec. V. Preliminary reports of this work can be found in [45–48].

## II. LATTICE SETUP

### A. Möbius domain-wall and overlap fermions

In this work, we employ the Möbius domain-wall fermion [37,38], which is numerically less expensive than the overlap fermion and allows topology tunneling at the cost of violating the Ginsparg-Wilson relation [35] at some small amount, which is controllable by the finite size $L_s$ of the fifth direction. This formulation is one of many possible implementations of lattice fermions satisfying the Ginsparg-Wilson relation. They are classified by the kernel operator and the approximation of the sign function. As described below, the Möbius domain-wall fermion has the same Shamir kernel $D_W/(2+D_W)$ [49,50], with $D_W$ the Wilson-Dirac operator, as that of the conventional domain-wall fermion [49–51], while improving the approximation of the sign function by introducing a scale parameter to the kernel. In this sense, the Möbius domain-wall fermion is a *better* domain-wall fermion. The overlap fermion formulation of Neuberger [39,40] has a different kernel, $D_W$, and

the rational approximation of the sign function is typically adopted. As far as the chiral symmetry of the resulting fermion is concerned, the difference of the kernels and the details of the sign function approximation are not important.

In the following, we take the lattice spacing $a = 1$ unless otherwise stated. It is shown that the fermion determinant generated with the domain-wall fermion together with the associated Pauli-Villars field is equivalent to a determinant of the four-dimensional (4D) effective operator [37,38],

$$D^{4D}_{\mathrm{DW}}(m) = \frac{1+m}{2} + \frac{1-m}{2}\gamma_5 \mathrm{sgn}(H_M). \tag{3}$$

Here, $m$ is the quark mass, and the matrix sign function "sgn" is approximated by

$$\mathrm{sgn}(H_M) = \frac{1-(T(H_M))^{L_s}}{1+(T(H_M))^{L_s}} \tag{4}$$

with the transfer matrix $T(H_M) = (1-H_M)/(1+H_M)$. The kernel operator $H_M$ is written as

$$H_M = \gamma_5 \frac{\alpha D_W}{2 + D_W}, \tag{5}$$

where $D_W$ is the Wilson-Dirac operator with a large negative mass $-1/a$. The scale parameter $\alpha$ is set to 2 in this work. This corresponds to the Möbius domain-wall fermion [38], while $\alpha = 1$ gives the standard domain-wall fermion. With this choice, the Ginsparg-Wilson relation is realized with a better precision at a fixed $L_s$. The sign function in (4) is equivalent to the form $\tanh(L_s \tanh^{-1}(H_M))$, which converges to the exact sign function in the limit $L_s \to \infty$. This is called the polar approximation. In this limit, the Ginsparg-Wilson relation is exactly satisfied. The details of our choice of the parameters are reported in [52].

The size of the violation of chiral symmetry for the Möbius domain-wall fermion may be quantified by the residual mass,

$$m_{\mathrm{res}} = \frac{\langle \mathrm{tr} G^\dagger \Delta_{\mathrm{GW}} G \rangle}{\langle \mathrm{tr} G^\dagger G \rangle}, \tag{6}$$

with

$$\Delta_{\mathrm{GW}} \equiv \frac{\gamma_5}{2}[D^{4D}_{\mathrm{DW}}(0)\gamma_5 + \gamma_5 D^{4D}_{\mathrm{DW}}(0) - 2a D^{4D}_{\mathrm{DW}}(0)\gamma_5 D^{4D}_{\mathrm{DW}}(0)], \tag{7}$$

where $G$ is the contact-term-subtracted quark propagator,

$$G = \frac{1}{1-m}((D^{4D}_{\mathrm{DW}}(m))^{-1} - 1). \tag{8}$$

We confirm that the residual mass of the Möbius domain-wall fermion as defined in (6) is roughly 5–10 times smaller than that of the standard domain-wall Dirac operator at the same value of $L_s$ [52].

Even when the residual mass calculated as (6) is small, at a level of a few MeV or less, the low-lying mode of $D^{4D}_{\mathrm{DW}}$ may be significantly affected by such small violation of the Ginsparg-Wilson relation [34]. In fact, it was shown that the contribution to the chiral condensate is in some cases dominated by the lattice artifact that violates the Ginsparg-Wilson relation. Since we are interested in the details of the low-mode spectrum, we need to carefully study such effects. For that reason, we introduce the overlap fermion (with the same kernel as the domain-wall fermion) and perform the reweighting to eliminate the contamination from the lattice artifact.

One may improve the sign function approximation in (3) by exactly treating the low-lying eigenmodes of the kernel operator $H_M$, since the polar approximation is worse for the low modes. We compute $N_{\mathrm{th}}$ lowest eigenmodes of the kernel operator $H_M$ and exactly calculate the sign function for this part of the spectrum. Namely, we define

$$D_{\mathrm{ov}}(m) = \sum_{|\lambda_i^M|<\lambda_{\mathrm{th}}^M} \left[\frac{1+m}{2} + \frac{1-m}{2}\gamma_5 \mathrm{sgn}(\lambda_i^M)\right] |\lambda_i^M\rangle\langle\lambda_i^M| + D^{4D}_{\mathrm{DW}}(m)\left[1 - \sum_{\lambda_i^M<|\lambda_{\mathrm{th}}^M|} |\lambda_i^M\rangle\langle\lambda_i^M|\right], \tag{9}$$

where $\lambda_i^M$ is the $i$th eigenvalue of $H_M$ nearest to zero and $\lambda_{\mathrm{th}}^M$ is a certain threshold. We choose $\lambda_{\mathrm{th}}^M = 400 - 600$ MeV depending on the parameters. With these choices, the violation of chiral symmetry is kept negligible, at the order of $\sim$1 eV in our ensembles.

In this paper, we slightly misuse the terminology and call thus defined $D_{\mathrm{ov}}$ the overlap-Dirac operator, though the kernel is that of domain-wall fermion, i.e., the Shamir kernel.

Since the difference between $D^{4D}_{\mathrm{DW}}$ and $D_{\mathrm{ov}}$ appears only in the treatment of the low modes of $H_M$, we expect a good overlap in their relevant configuration spaces and a mild fluctuation of the reweighting factor between them. This is indeed the case for the $16^3 \times 8$ and $32^3 \times 12$ lattices we generated using $D^{4D}_{\mathrm{DW}}$, as we will see below.

### B. Configuration generation

For the gauge part, we use the tree-level improved Symanzik gauge action [53]. We apply the stout smearing [54] 3 times on the gauge links with the $\rho$ parameter $\rho = 0.1$ before computing the Dirac operators. All the details on the choice of the parameters for these actions are reported in our zero temperature studies [55,56].

Our simulation setup is summarized in Table I. The lattice spacing $a$ is estimated by the Wilson flow on a few

TABLE I. Summary of simulated ensembles. The residual mass $m_{\rm res}a$ is calculated using the definition (6). #trj denotes the number of trajectories. $N_{\rm conf}$ presents the number of configurations generated (those with parenthesis are not used in the main analysis of this work but used for the estimate of the critical temperature). $N_{\rm conf}^{\rm eff}$ and $N_{\rm conf}^{\rm eff(2)}$ are the effective statistics after the overlap/domain-wall reweighting, which are defined by (15) and (16) (data with * are measured by a low-mode approximation of the reweighting). $\tau_{\rm int}^{\rm CG}$ and $\tau_{\rm int}^{\rm top}$ are the integrated autocorrelation time of the CG iteration count and topological charge, respectively, in the units of the molecular dynamics time. $M_{PS}L$ is the screening mass of the pseudoscalar correlator multiplied by the lattice size $L$.

| $L^3 \times L_t$ | $\beta$ | $ma$ | $L_s$ | $m_{\rm res}a$ | $T$ [MeV] | #trj | $N_{\rm conf}$ | $N_{\rm conf}^{\rm eff}$ | $N_{\rm conf}^{\rm eff(2)}$ | $\tau_{\rm int}^{\rm CG}$ | $\tau_{\rm int}^{\rm top}$ | $M_{PS}L$ |
|---|---|---|---|---|---|---|---|---|---|---|---|---|
| $16^3 \times 8$ | 4.07 | 0.01 | 12 | 0.00166(15) | 203(1) | 6600 | 239 | 11(13) | 45(8) | 70 | 25(6) | 5.4(3) |
| $16^3 \times 8$ | 4.07 | 0.001 | 24 | 0.00097(43) | 203(1) | 12000 | 197 | 7(7) | 14(3) | 315 | 23(4) | 5.3(4) |
| $16^3 \times 8$ | 4.10 | 0.01 | 12 | 0.00079(5) | 217(1) | 7000 | 203 | 23(7) | 150(17) | 134 | 30(10) | 6.9(5) |
| $16^3 \times 8$ | 4.10 | 0.001 | 24 | 0.00048(14) | 217(1) | 12000 | 214 | 31(10) | 121(10) | 104 | 24(4) | 6.3(9) |
| $32^3 \times 8$ | 4.07 | 0.001 | 24 | 0.00085(9) | 203(1) | 4200 | 210 | 10(3)* | ··· | 128 | 18(4) | 11.7(9) |
| $32^3 \times 8$ | 4.10 | 0.01 | 12 | 0.0009(5) | 217(1) | 3800 | 189 | 9(4)* | ··· | 125 | 30(10) | 12.6(5) |
| $32^3 \times 8$ | 4.10 | 0.005 | 24 | 0.00053(4) | 217(1) | 3100 | 146 | 20(4)* | ··· | 84 | 24(9) | 11.6(7) |
| $32^3 \times 8$ | 4.10 | 0.001 | 24 | 0.00048(5) | 217(1) | 7700 | 229 | 18(5)* | ··· | 10 | 23(5) | 12.3(9) |
| $32^3 \times 12$ | 4.18 | 0.01 | 16 | 0.00022(5) | 172(1) | 2600 | (319) | ··· | ··· | ··· | ··· | 5.8(1) |
| $32^3 \times 12$ | 4.20 | 0.01 | 16 | 0.00020(1) | 179(1) | 3400 | (341) | ··· | ··· | ··· | ··· | ··· |
| $32^3 \times 12$ | 4.22 | 0.01 | 16 | 0.00010(1) | 187(1) | 7000 | (703) | ··· | ··· | ··· | ··· | 5.4(2) |
| $32^3 \times 12$ | 4.23 | 0.01 | 16 | 0.00008(1) | 191(1) | 5600 | 51 | 28(4) | 38(5) | 240 | 120(50) | ··· |
| $32^3 \times 12$ | 4.23 | 0.005 | 16 | 0.00012(1) | 191(1) | 10300 | 206 | 22(2) | 27(2) | 131 | 160(140) | ··· |
| $32^3 \times 12$ | 4.23 | 0.0025 | 16 | 0.00016(4) | 191(1) | 9400 | 195 | 16(2) | 255(31) | 85 | 110(30) | ··· |
| $32^3 \times 12$ | 4.24 | 0.01 | 16 | 0.00008(1) | 195(1) | 7600 | 49 | 23(5) | 36(5) | 125 | 100(40) | 6.8(5) |
| $32^3 \times 12$ | 4.24 | 0.005 | 16 | 0.00010(2) | 195(1) | 9700 | 190 | 9(18) | 53(6) | 84 | 130(30) | ··· |
| $32^3 \times 12$ | 4.24 | 0.0025 | 16 | 0.00011(2) | 195(1) | 16000 | 188 | 8(10) | 7(1) | 618 | 80(20) | 6(2) |

selected zero-temperature configurations. We use the reference flow time $t_0 = (0.1539\ \text{fm})^2$ determined by the ALPHA Collaboration [57] for $N_f = 2$ QCD. The results at different quark masses are extrapolated to the chiral limit, and the data are interpolated in $\beta$ assuming perturbative running [58–62],

$$a = c_0 f(g^2)(1 + c_2 \hat{a}(g)^2), \qquad \hat{a}(g)^2 \equiv [f(g^2)]^2,$$
$$f(g^2) \equiv (b_0 g^2)^{-b_1/2b_0^2} \exp\left(-\frac{1}{2b_0 g^2}\right),$$
$$b_0 = \frac{1}{(4\pi)^2}\left(11 - \frac{2}{3}N_f\right), \qquad b_1 = \frac{1}{(4\pi)^4}\left(102 - \frac{38N_f}{3}\right), \tag{10}$$

where $g^2 = 6/\beta$, $N_f = 2$, and $c_0$ and $c_2$ are free parameters of the fit. The result is plotted in Fig. 1 with our estimates $c_0 = 6.9(2)$ and $c_2 = 6.1(6) \times 10^3$. The simulated lattice spacing covers the range between 0.074 fm ($\beta = 4.30$) and 0.127 fm ($\beta = 4.05$). Our estimates of the temperature on $L_s = 8$ and 12 lattices are listed in Table I.

We estimate the critical temperature as $T_c = 175(5)$ MeV from the inflection point of the Polyakov loop, as shown in Fig. 2. We confirm that the ensembles listed in Table I are at or above the chiral phase transition.

The physical lattice size $L$ is 2–4 fm in the spatial directions. We confirm by the calculation of the pseudoscalar correlators that the correlation length in the spatial direction $1/M_{PS}$ is sufficiently small compared to the spatial lattice size $L$. The values of $M_{PS}L$ are listed in Table I. We also present some effective mass plots in Fig. 3. Because of a small correlation length of the finite temperature system, no significant finite volume effects are expected even for those ensembles at smallest quark masses.

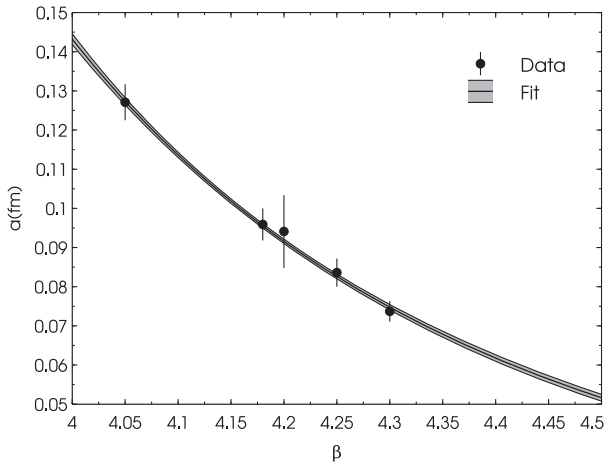


FIG. 1. Lattice spacing $a$ as a function of $\beta$, for the choice of lattice action in this work, estimated using the Wilson flow scale $t_0$. The data are interpolated by a perturbative prediction given in (10). The band represents the error in the estimate, which is negligible (<0.5%) for the ensembles discussed in this work.

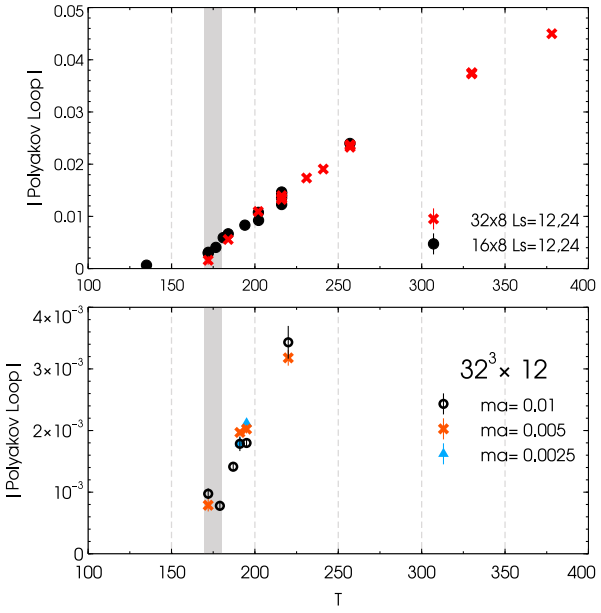


FIG. 2. The Polyakov loop expectation value as a function of temperature. The results for $L_t = 8$ (top panel) and those for $L_t = 12$ (bottom) are shown. The critical temperature $T_c$ is estimated as 175(5) MeV, which is shown by a shadow band.

The bare quark mass is chosen in the range from 2 to 25 MeV. The residual mass (6) in our simulations is $\lesssim 1$ MeV around $T_c$ and even smaller at higher temperature. We have data at two values of $L_s = 8$ and 12 to check the discretization effects.

The ensembles are generated with the standard hybrid Monte-Carlo method. We estimate the autocorrelation time using the conjugate gradient (CG) iteration number in the inversion of the fermion matrix. Depending on ensembles, it is around 70–600 in the unit of the molecular dynamics time. Statistical error is estimated using the jackknife method with the bin size greater than the integrated autocorrelation time of the observable. The number of measurement is $O(100)$ depending on the ensemble as listed in the column of #conf. Each measurement is separated by 20–100 molecular dynamics time.

In order to check whether the topology tunneling frequently occurs in our simulations, we monitor the topological charge $Q$ of each configuration. Here, we use the field theoretical definition for $Q$

$$Q = \frac{1}{32\pi^2}\sum_x \epsilon^{\mu\nu\rho\sigma}\mathrm{Tr}F_{\mu\nu}(x)F_{\rho\sigma}(x), \tag{11}$$

where the field strength $F_{\mu\nu}$ is defined using the clover leaf construction, measured after the Wilson flow [63] of its flow time $ta^2 \simeq 5$ (the measurement of $Q$ is stable for $ta^2 \gtrsim 3$). We confirm that it changes frequently along the simulations. One example is shown in Fig. 4. The autocorrelation time for the topological charge is also listed in Table I.

For the configurations generated, we compute the low-lying eigenvalues of the 4D Hermitian effective operators $H_{\mathrm{DW}}^{\mathrm{4D}}(m) \equiv \gamma_5 D_{\mathrm{DW}}^{\mathrm{4D}}(m)$ and $H_{\mathrm{ov}}(m) \equiv \gamma_5 D_{\mathrm{ov}}(m)$ using the implicitly restarted Lanczos algorithm with $O(100)$ Krylov vectors [64]. From the eigenvalues of $H_{\mathrm{ov}}(m)$, we can also extract the number of chiral zero modes $n_+$ with positive chirality and $n_-$ with negative chirality. For each zero mode of $D_{\mathrm{ov}}(0)$ with $\pm$ chirality, we have a mode whose eigenvalue of $H_{\mathrm{ov}}(m)$ is $\pm m$. Since these zero modes are generally isolated, while other nonzero modes make $\pm\lambda^{(m)}$ pairs, our numerical determination of $n_+$ and $n_-$ is quite robust, and thus, we can determine the topological index $\nu = n_+ - n_-$ of the overlap Dirac operator, as well as the number of the zero modes $N_0 = n_+ + n_-$.

### C. Overlap/domain-wall reweighting

The expectation value of an observable $\mathcal{O}$ with the dynamical overlap fermion can be estimated by the reweighting as

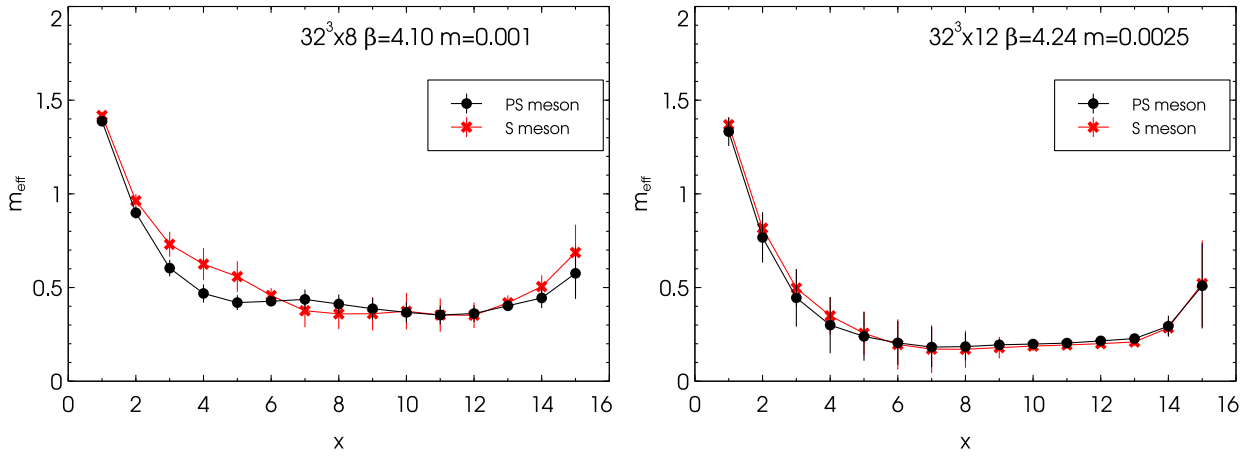


FIG. 3. Effective mass plots of the spatial correlator at $\beta = 4.10$, $m = 0.001$ on the $32^3 \times 8$ lattice (left panel), and those at $\beta = 4.24$, $m = 0.0025$ on the $32^3 \times 12$ lattice (right). The correlation functions in the pseudoscalar (black) and scalar (red) channels are shown.

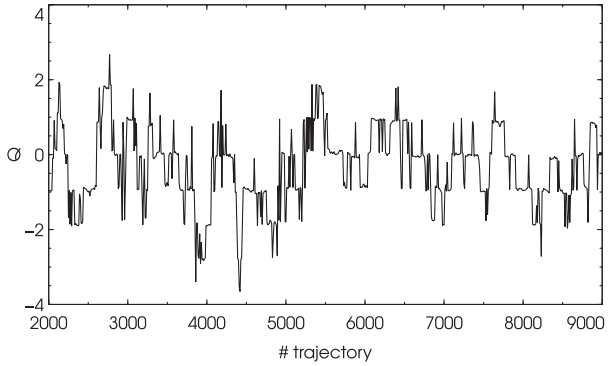


FIG. 4. History of the topological charge for $L^3 \times L_t = 32^3 \times 12$, $\beta = 4.24$, $m = 0.01$.

$$\langle \mathcal{O} \rangle_{\rm ov} = \frac{\langle \mathcal{O}R \rangle_{\rm DW}}{\langle R \rangle_{\rm DW}}, \tag{12}$$

where $\langle \cdots \rangle_{\rm DW}$ and $\langle \cdots \rangle_{\rm ov}$ denotes the ensemble average with the Möbius domain wall and overlap sea quarks, and $R$ is the reweighting factor

$$R \equiv \frac{\det[H_{\rm ov}(m)]^2}{\det[H_{\rm DW}^{\rm 4D}(m)]^2} \times \frac{\det[H_{\rm DW}^{\rm 4D}(1/4a)]^2}{\det[H_{\rm ov}(1/4a)]^2}. \tag{13}$$

The second factor $\det[H_{\rm DW}^{\rm 4D}(1/4a)]^2/\det[H_{\rm ov}(1/4a)]^2$ in (13) is introduced to cancel the noise from high modes at the cutoff scale [65]. It corresponds to adding fermions and ghosts of a cutoff scale mass $1/4a$, and therefore does not affect the low-energy physics we are interested in. The reweighting factor is stochastically estimated [66] with Gaussian noise fields $\xi_i$ and $\xi_i'$,

$$R = \frac{1}{N}\sum_{i=1}^{N} \exp[-\xi_i^\dagger [H_{\rm DW}^{\rm 4D}(m)]^2 [H_{\rm ov}(m)]^{-2} \xi_i - \xi_i'^\dagger [H_{\rm DW}^{\rm 4D}(1/2a)]^{-2} [H_{\rm ov}(1/2a)]^2 \xi_i'], \tag{14}$$

with a few noise samples for each configuration.

The reweighting is effective when the factor $R$ does not fluctuate too much. Since the factor scales exponentially as a function of the volume of the lattice, the relevant matrix $[H_{\rm DW}^{\rm 4D}(m)]^2[H_{\rm ov}(m)]^{-2}$ needs to be close to an identity operator. Our operator $D_{\rm ov}(m)$ is designed to satisfy this condition, i.e., only the treatment of the near-zero eigenmodes of the kernel operator is different. It is however not known how such difference affects $R$ until we actually compute it. Figure 5 shows examples of the Monte Carlo history of $R$. It turns out that the maximum of $R$ is at the level of $O(10)$ on $16^3 \times 8$ and $32^3 \times 12$ lattices, which does not destroy the ensemble average when we have $O(100)$ samples. To assess the quality of the reweighting, we define the effective number of configurations [67] by

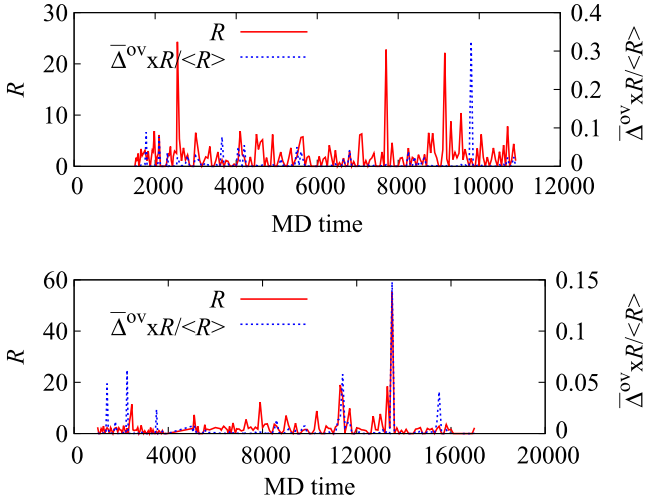


FIG. 5. History of the reweighting factor $R$ (solid) and that of $\bar{\Delta}^{\rm ov}_{\pi-\delta} \times R/\langle R \rangle$ (dashed) for $L^3 \times L_t = 32^3 \times 12$ ensembles at $\beta = 4.23$ (top), 4.24 (bottom) with the same bare quark mass $m = 0.0025$. The definition of $\bar{\Delta}^{\rm ov}_{\pi-\delta}$ is given by Eq. (24).

$$N_{\rm conf}^{\rm eff} = \frac{\langle R \rangle}{R_{\rm max}}, \tag{15}$$

where $R_{\rm max}$ is the maximum value of the reweighting factor in the ensemble. However, as shown in the same plot in Fig. 5, it turns out that $R_{\rm max}$ does not necessarily coincide with the peak of the observable $\mathcal{O}R$, e.g., $\mathcal{O} = \bar{\Delta}^{\rm ov}_{\pi-\delta}$ as defined later. Therefore, we also measure

$$N_{\rm conf}^{\rm eff(2)} = \frac{\langle R \rangle}{R'_{\rm max}}, \tag{16}$$

with $R'_{\rm max}$ the reweighting factor which gives the maximum value of $\bar{\Delta}^{\rm ov}_{\pi-\delta} \times R$ in the ensemble. Both $N_{\rm conf}^{\rm eff}$ and $N_{\rm conf}^{\rm eff(2)}$ are listed in Table I. $N_{\rm conf}^{\rm eff(2)}$ is larger than $N_{\rm conf}^{\rm eff}$ except for the configurations at $\beta = 4.24$ and $m = 0.0025$.

In particular, on the $16^3 \times 8$ lattices, the reweighting factors are stable enough that we can choose different quark masses from that of the original ensemble: $m = 0.005$ on $m = 0.01$ Möbius domain-wall ensembles.

There are some configurations for which the reweighting factor is essentially zero, say $R < 10^{-3}$. For these configurations, we find chiral zero modes for the overlap-Dirac operator. They are suppressed as the fermion determinant contains a factor $(am)^2$ from the zero mode, and the next lowest eigenvalues are also smaller compared to the corresponding eigenvalues of the Möbius domain-wall Dirac operator. We note that the pairing of the positive and negative eigenvalues of $H_{\rm ov}$ is precisely satisfied other than the exact zero modes. With $H_{\rm DW}^{\rm 4D}$, such correspondence is hardly visible especially for the coarser lattices at $L_t = 8$.

For the large-volume lattices of size $32^3 \times 8$, we found that the reweighting as described above are not effective.

TABLE II. Polyakov loop for original configurations $\langle L\rangle$ and the reweighted one $\langle L\rangle_{\rm rew}$. Here, coarser lattice data are for $L^3 = 16^3$.

| $\beta$ | $am_{\rm ud}$ | $\langle L\rangle$ | $\langle L\rangle_{\rm rew}$ |
|---|---|---|---|
| 4.07 | 0.01 | 0.01032 (45) | 0.01023 (18) |
| 4.07 | 0.001 | 0.01147 (27) | 0.0117 (15) |
| 4.10 | 0.01 | 0.01457 (34) | 0.0141 (13) |
| 4.10 | 0.001 | 0.01294 (45) | 0.0130 (11) |
| 4.23 | 0.01 | 0.00225 (16) | 0.00254 (54) |
| 4.23 | 0.005 | 0.00495 (75) | 0.00435 (92) |
| 4.23 | 0.0025 | 0.00262 (23) | 0.00235 (57) |
| 4.24 | 0.01 | 0.00233 (18) | 0.00245 (77) |
| 4.24 | 0.005 | 0.00788 (61) | 0.0076 (13) |
| 4.24 | 0.0025 | 0.00400 (48) | 0.00367 (75) |

On these lattices, the lattice spacing is relatively large, $a \simeq 0.11$ fm, and the difference between $D^{\rm 4D}_{\rm DW}$ and $D_{\rm ov}$ is more significant. With a larger spatial volume, such a difference is enhanced exponentially. For these lattices, we introduce a reweighting scheme that takes only the low-mode part of the eigenvalue spectrum. Namely, we approximate the reweighting factor by

$$R_{\rm low} = \frac{\prod_{k=1}^{N_{th}} (\lambda^{(m)}_{{\rm ov},k})^2}{\prod_{k=1}^{N_{th}} (\lambda^{(m)}_{{\rm DW},k})^2}, \tag{17}$$

where $\lambda^{(m)}_{{\rm ov},k}$ and $\lambda^{(m)}_{{\rm DW},k}$ denote the $k$th lowest eigenvalue of the Hermitian operators $H_{\rm ov}(m)$ and $H^{\rm 4D}_{\rm DW}(m)$, respectively. The number of the eigenvalues included $N_{th}$ is 40 except for $N_{th} = 10$ at $\beta = 4.10$ and $m = 0.01$. The threshold is around $0.1/a \sim 160$ MeV.

The low-mode reweighting (17) corresponds to introducing an extra ultraviolet modification to the fermion determinant ratio (13). However, its modification does not distort the continuum limit since $D^{\rm 4D}_{\rm DW}$ precisely converges to $D_{\rm ov}$ in that limit as the probability of having low-lying modes of $2H_M$ less than $\lambda^M_{\rm th}$ vanishes. Namely, both $R$ and $R_{\rm low}$ are guaranteed to converge to unity in the continuum limit and share the same continuum limit. We confirm on the small $16^3 \times 8$ lattice, where the full reweighting is available, that $R$ and $R_{\rm low}$ give consistent results for the Dirac spectrum. We also confirm that our observable for the $U(1)_A$ symmetry breaking is dominated by the lowest modes much below the threshold of $0.1/a$, as will be discussed in Sec. IV.

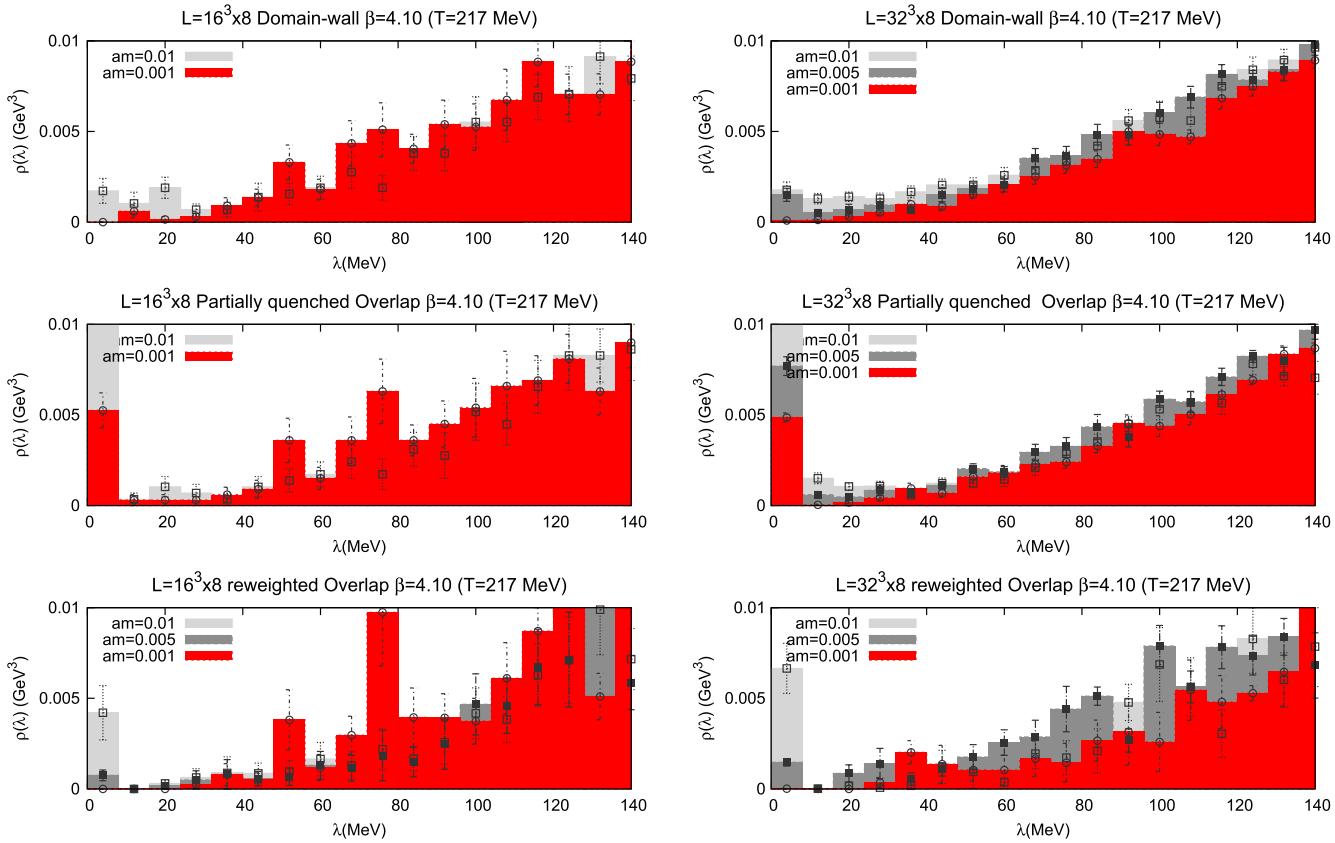


FIG. 6. Eigenvalue spectrum of the Möbius domain wall (top panels), partially quenched overlap with Möbius domain-wall sea quarks (middle), and the (reweighted) overlap (bottom) Dirac operators. Data at $\beta = 4.10$ ($T \sim 217$ MeV) on $16^3 \times 8$ (left panels) and $32^3 \times 8$ (right) are shown. The data for $m = 0.005$ on the $16^3 \times 8$ lattice are obtained by reweighting on the $m = 0.01$ ensemble.

As will be shown below, our target of this work, $U(1)_A$ sensitive quantities, are sensitive to the overlap/Domain-wall reweighting. However, the reweighting does not affect those insensitive to the $U(1)_A$ symmetry. For example, we find that the plaquette changes only by less than 0.3%, which is much smaller than its statistical error (of reweighted plaquettes). Table II is a comparison of the Polyakov loop with and without the reweighting. This table shows that for $U(1)_A$ insensitive quantities, the overlap fermions and Möbius domain-wall fermions are essentially the same.

## III. DIRAC SPECTRUM

In this section, we study the Dirac spectrum $\rho(\lambda)$, which is tightly related to both of the $SU(2)_L \times SU(2)_R$ and $U(1)_A$ symmetries [68]. We compute the eigenvalues $\lambda_k^{(m)}$ of the massive operators $H_{\mathrm{DW}}^{4\mathrm{D}}(m)$ and $H_{\mathrm{ov}}(m)$, and evaluate those of the massless operators using

$$\lambda_k = \frac{\sqrt{(\lambda_k^{(m)})^2 - m^2}}{\sqrt{1-m^2}}. \tag{18}$$

When the Ginsparg-Wilson relation is satisfied, $\lambda_k$ is exactly the same as the corresponding eigenvalue of the massless Dirac operator. We apply the same formula to the Möbius domain-wall Dirac eigenvalues, though the Ginsparg-Wilson relation is not exact. We confirm that $|\lambda_k^{(m)}| > m$ is always satisfied, and the effect of $m_{\mathrm{res}}$ is invisible with our resolution of the Dirac eigenvalue density explained below.

Figure 6 shows the eigenvalue histograms of the Möbius domain wall (top panels), partially quenched overlap with Möbius domain-wall sea quarks (middle), and (reweighted) overlap (bottom) Dirac operators. Data at $\beta = 4.10$ ($T \sim 217$ MeV) on the $16^3 \times 8$ lattice are shown on the left panels, and those on the $32^3 \times 8$ lattice are shown on the right panels. Here, we count the number of eigenvalues in a bin $[\lambda - 4\mathrm{MeV}, \lambda + 4\mathrm{MeV}]$ and rescale them by $1/V$ to obtain the eigenvalue density $\rho(\lambda)$ in the physical unit. When the data for different sea quark masses are plotted together, the heavier mass data are shown by shaded histograms. When there are exactly chiral zero modes, they are included in the lowest bin.

The Möbius domain-wall Dirac operator spectrum shows a mild slope towards zero at the lightest quark masses near the chiral limit. This slope is consistent with $\lambda^3$, which was also reported in [28] employing the optimal domain-wall fermions. The reweighted overlap Dirac operator

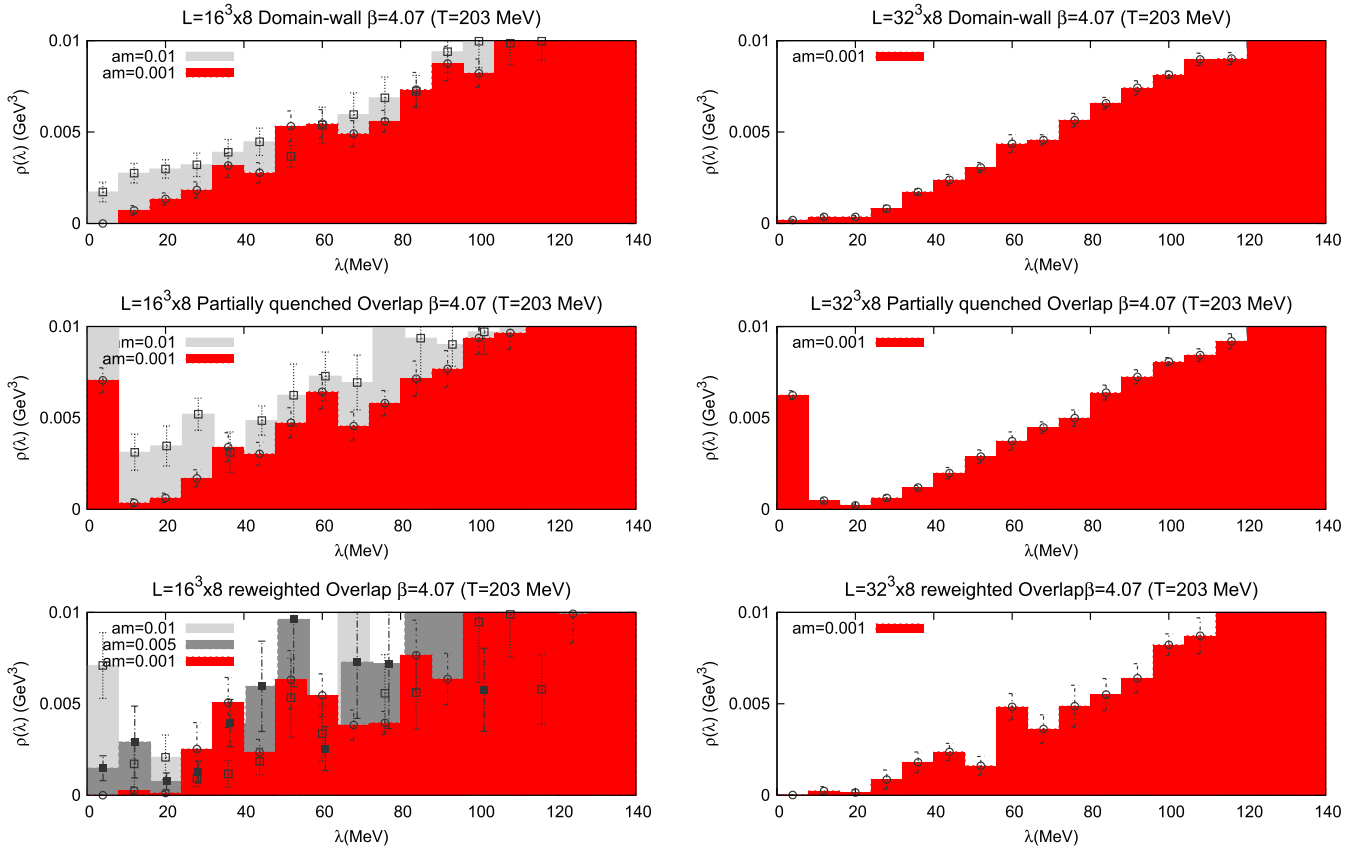


FIG. 7. Same as Fig. 6 but at $\beta = 4.07$ ($T \sim 203$ MeV).

histograms look similar but we can see a stronger suppression of the near zero modes: the first three bins are consistent with zero, which is consistent with our previous work [27].

In contrast to a qualitative agreement of the Möbius domain wall and overlap Dirac operators, a striking difference is seen in the data for the partially quenched overlap or the overlap Dirac spectrum without reweighting: a sharp peak is found at the lowest bin, which does not disappear even at the lightest quark mass. The appearance of such a peak structure, mainly coming from the chiral zero modes, is known from previous works with overlap fermions on pure gauge configurations (see, e.g., [27]). Recently, a similar structure was reported in the overlap Dirac spectrum on the ensembles generated by the HISQ action [33]. Since such a peak does not appear in the Möbius domain wall and reweighted overlap eigenvalues, they are likely an artifact of partial quenching.

The above properties of the Dirac eigenvalue spectrum are insensitive to the volume and lattice spacing, as presented in Figs. 7 and 8. We emphasize that the strong suppression of the near-zero modes does not change even when we vary the lattice volume size from 2 fm to 4 fm, where the latter volume is 8 times larger than the former. If there were a (pseudo)gap due to the finite volume, it should scale as a power of $1/L$. We also confirm that the screening mass in the pseudoscalar channel $M_{PS}$ is large enough to satisfy $M_{PS}L > 5$, and the finite volume effects are well under control.

We also remark that our data at the lowest bin, or the eigenvalue density below 8 MeV, show a monotonically decreasing quark mass dependence, as presented in Fig. 9. Both data of the Möbius and overlap Dirac operators at $m < 5$ MeV are consistent with zero.

Since the difference between the Möbius domain wall and the reweighted overlap Dirac spectra are not clear, one may think that they are qualitatively the same, and the overlap/domain-wall reweighting is not needed for the analysis of the $U(1)_A$ susceptibility. However, as we already reported in [34,70], we found a significant difference in the chiral symmetry of the individual eigenmodes of the two Dirac operators. In [34], we investigated the effects of chiral symmetry violation, or violation of the Ginsparg-Wilson relation on each eigenmode, and how they affect the physical observables. For example, we observed

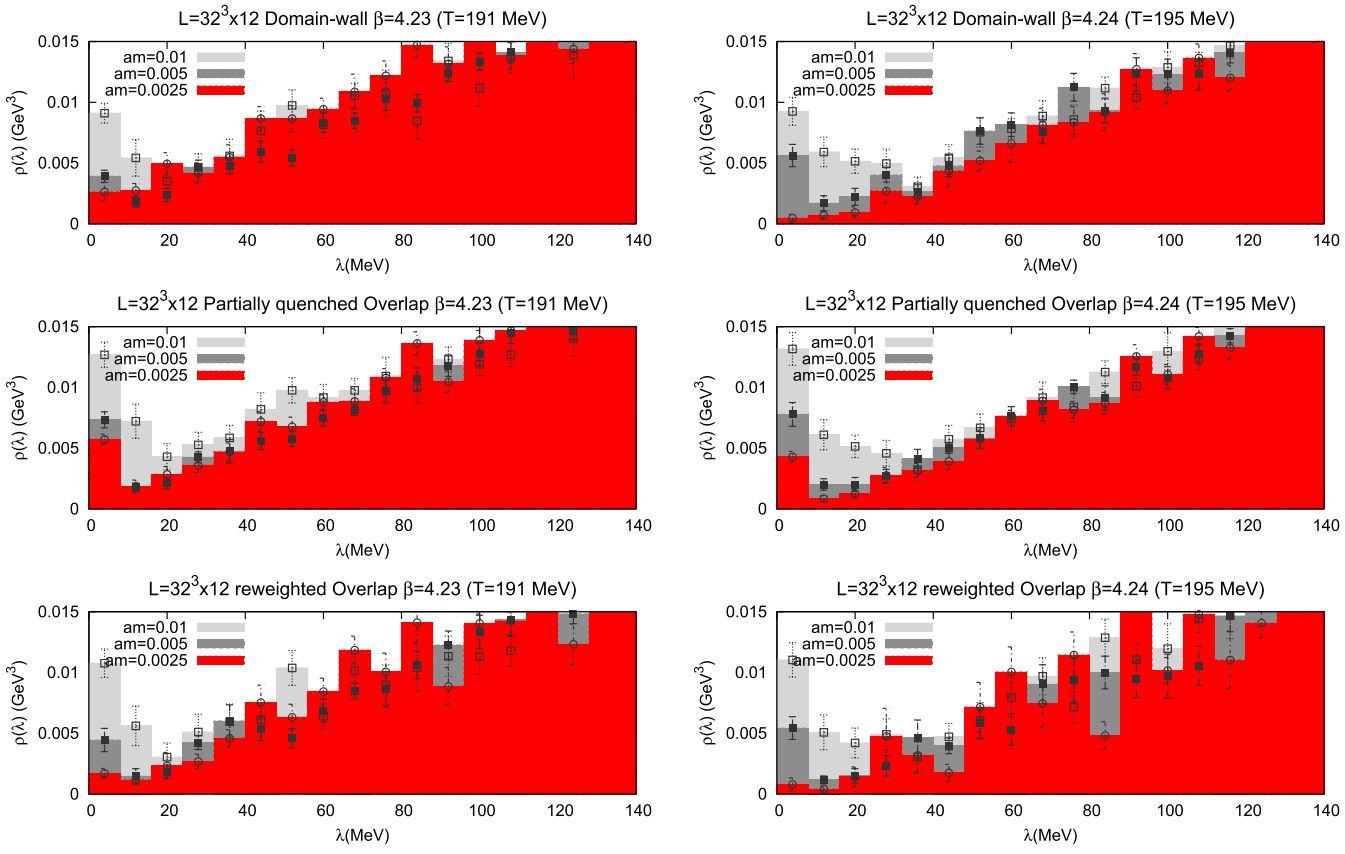


FIG. 8. Same as Fig. 6 but on finer lattices. Data at $\beta = 4.23$ ($T \sim 191$ MeV) (left panel) and at $\beta = 4.24$ ($T \sim 195$ MeV) (right) on the $32^3 \times 12$ lattice are plotted.

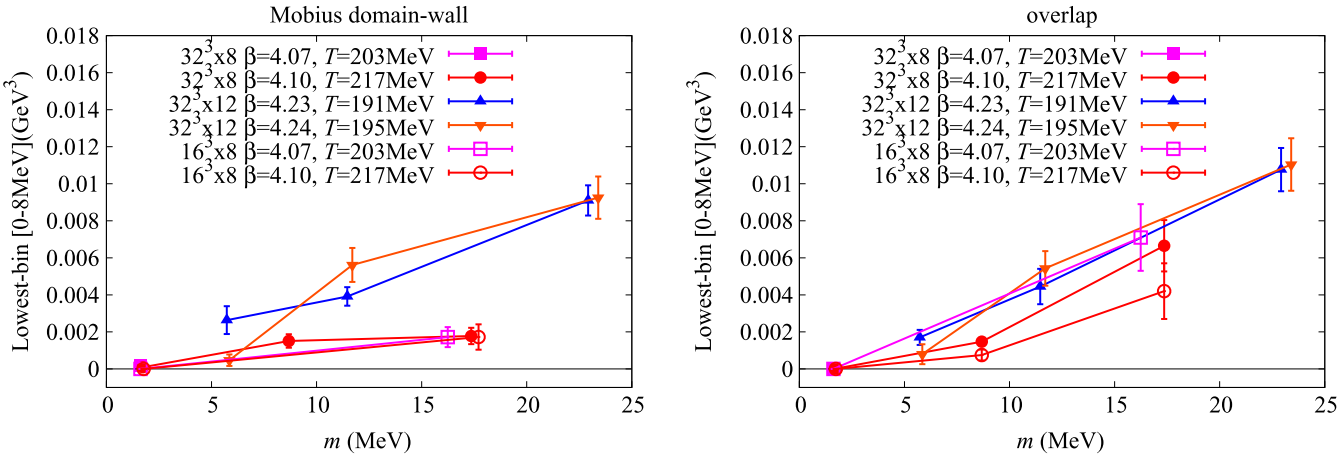


FIG. 9. The quark mass dependence of the eigenvalue density at the first bin [0,8] MeV. The data of the Möbius domain wall (left panel) and those of the overlap (right) Dirac operators are shown. All the data for $m < 5$ MeV are consistent with zero.

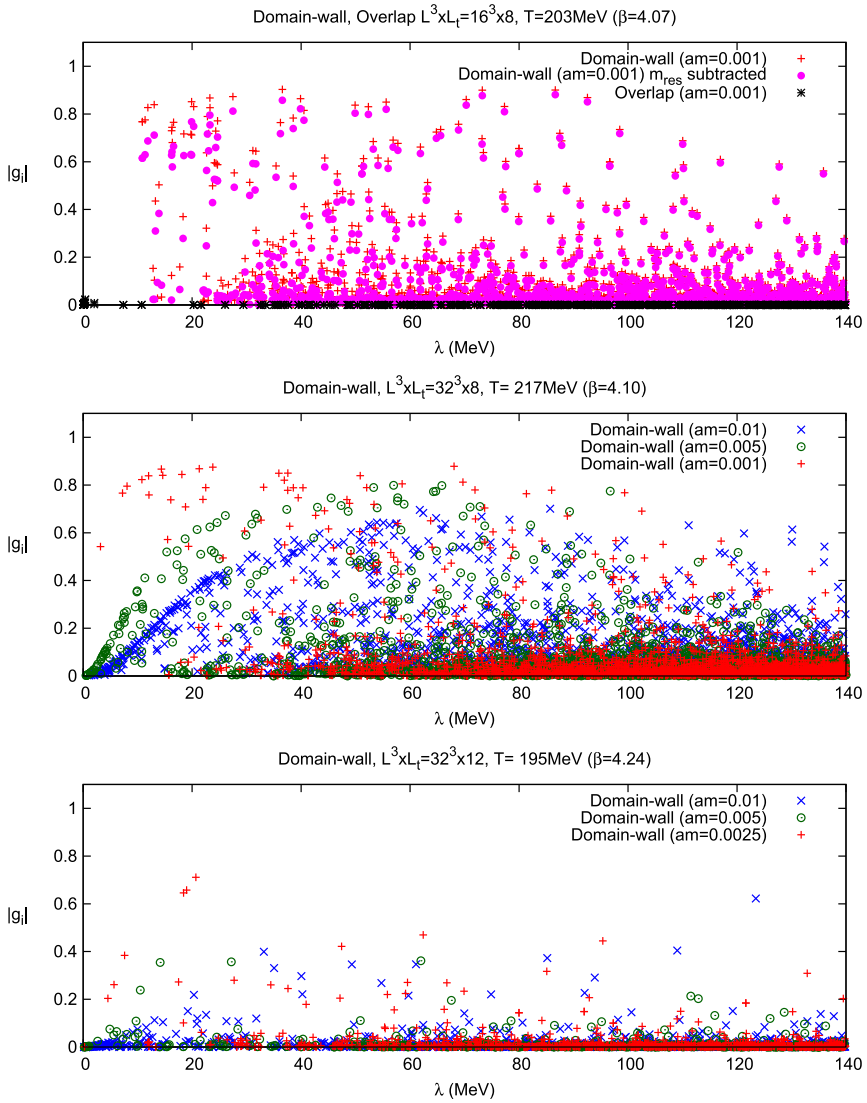


FIG. 10. Violation of the Ginsparg-Wilson relation $g_i$ as measured for individual eigenmodes. Data for $\beta = 4.07$ on a $L^3 \times L_t = 16^3 \times 8$ lattice (top panel), those for $\beta = 4.10$ and $L^3 \times L_t = 32^3 \times 8$ (middle), and those for $\beta = 4.24$ and $L^3 \times L_t = 32^3 \times 12$ (bottom) are shown. Results for all the measured configurations are plotted.

$$g_i \equiv \frac{\psi_i^\dagger \Delta_{\rm GW} \psi_i}{\lambda_i^{(m)}} \left[\frac{(1-am)^2}{(1+am)}\right], \tag{19}$$

where $\Delta_{\rm GW}$ is defined by (7), and $\lambda_i^{(m)}$, $\psi_i$ denote the $i$th eigenvalue/eigenvector of massive Hermitian Dirac operator, respectively. The last factor in (19) comes from the normalization of the Dirac operator. $g_i$ vanishes when the Ginsparg-Wilson relation is exactly satisfied.

As shown in Fig. 10, we found that the low-lying modes of the Möbius domain-wall Dirac operator (cross symbols) violate the chiral symmetry to the order of one, which means that the expectation value of the violation of the Ginsparg-Wilson relation is comparable to the eigenvalue $\lambda_i^{(m)}$ itself. On the top panel of Fig. 10, we also plotted the data using $D_{\rm DW}^{4D}(-m_{\rm res})$ (solid circles) instead of $D_{\rm DW}^{4D}(0)$, expecting some cancellation with the effect from the residual mass [72]. The improvement is at most 20%, and the violation remains to be $\mathcal{O}(1)$. For the overlap Dirac operator (star symbols on the top panel), $g_i$ is negligibly small, as expected.

This large violation of chiral symmetry may potentially distort the physical observables, if they are sensitive to these low-lying modes and their chirality. As will be shown in the next section (and it is discussed in detail in [34]), we find that at our lightest simulated mass, 60%–90% of the $U(1)_A$ susceptibility measured by the Möbius domain-wall Dirac fermions comes from the violation of the Ginsparg-Wilson relation.

The violation of the Ginsparg-Wilson relation on the low-lying modes of the Möbius domain-wall Dirac operator explains the large difference between the partially quenched and the reweighted overlap fermions. Not only the valence fermions but also sea fermions are required to satisfy a good chirality; otherwise, the physical observables can be largely distorted. Therefore, the overlap/domain-wall reweighting is essential in our analysis.

## IV. $U(1)_A$ SUSCEPTIBILITY

In this section, we directly investigate the $U(1)_A$ anomaly at high temperature by computing the susceptibility $\Delta_{\pi-\delta}$ in (1), which is obtained from the two-point correlators in the isotriplet scalar and pseudoscalar channels. These correlators are related by the $U(1)_A$ symmetry, and their difference must vanish when the symmetry is recovered. The use of the isotriplet channels has a practical advantage of not including disconnected diagrams, which are numerically demanding. In the previous work by the JLQCD Collaboration using dynamical overlap fermions [27], we measured the meson correlators at a finite temperature and found that at temperatures close to the phase transition, the mesons correlators coincide in the limit of small bare quark masses. Here, we reexamine the $U(1)_A$ anomaly having a better control of systematic errors from finite volumes and finite lattice spacings.

First, we examine how much the low-lying modes of the Dirac operator contribute to $\Delta_{\pi-\delta}$. The strong violation of the chiral symmetry in the low-lying modes, found in the previous section, may affect the results. We compare the eigenvalue decomposition of $\Delta_{\pi-\delta}$ (at finite $m$) with $N_{\rm ev} =$ 20–100 lowest eigenmodes of the Möbius domain-wall Dirac operator, $\Delta_{\pi-\delta}^{\rm ev}$, and that directly computed by inverting the Dirac operator, $\Delta_{\pi-\delta}^{\rm direct}$, with a stochastic average of the source points. This source point averaging is essential since our data at each single source point are noisy. We find that the lowest modes below $\lambda \sim 0.1/a$ are enough to saturate the signals on all simulated ensembles.

TABLE III. Summary of results. The data with the subscript "ov" denote those with reweighted overlap fermions, otherwise, those with Möbius domain-wall fermions. The results at $\beta = 4.10$, $m = 0.005$ on the $16^3 \times 8$ lattice (for which the asterisk is put) are obtained by choosing $m = 0.005$ for the overlap Dirac operator to reweight the Möbius domain-wall ensemble generated with $m = 0.01$.

| $L^3 \times L_t$ | $\beta$ | $m$ | $\rho_{\rm ov}$(0–8 MeV) | $\Delta_{\pi-\delta}^{\rm direct} a^2$ | $\Delta_{\pi-\delta}^{\rm ev} a^2$ | $\Delta_{\pi-\delta}^{\rm GW}/\Delta_{\pi-\delta}^{\rm ev}$ | $\Delta_{\pi-\delta}^{\rm ov} a^2$ | $\bar{\Delta}_{\pi-\delta}^{\rm ov} a^2$ |
|---|---|---|---|---|---|---|---|---|
| $16^3 \times 8$ | 4.07 | 0.01 | 0.0071(18) | 0.132(14) | 0.139(12) | 0.37(2) | 0.19(5) | 0.032(13) |
| $16^3 \times 8$ | 4.07 | 0.001 | $3(3) \times 10^{-12}$ | 0.032(7) | 0.0498(14) | 0.982(2) | 0.00015(5) | $1.5(6) \times 10^{-4}$ |
| $16^3 \times 8$ | 4.10 | 0.01 | 0.0042(15) | 0.073(12) | 0.064(11) | 0.278(40) | 0.074(19) | 0.012(6) |
| $16^3 \times 8$ | 4.10 | 0.005* | 0.0008(3) | 0.009(2) | ⋯ | ⋯ | 0.0003(1) | 0.003(1) |
| $16^3 \times 8$ | 4.10 | 0.001 | $1.5(1.5) \times 10^{-8}$ | 0.017(8) | 0.0232(13) | 0.983(4) | $6(3) \times 10^{-5}$ | $6(3) \times 10^{-5}$ |
| $32^3 \times 8$ | 4.07 | 0.001 | 0.00002(1) | 0.105(32) | 0.105(35) | 0.65(10) | 0.03(2) | −0.004(3) |
| $32^3 \times 8$ | 4.10 | 0.01 | 0.0067(14) | 0.076(5) | 0.069(5) | 0.30(2) | 0.120(24) | 0.065(29) |
| $32^3 \times 8$ | 4.10 | 0.005 | 0.00147(20) | 0.111(16) | 0.107(15) | 0.17(2) | 0.111(34) | 0.025(9) |
| $32^3 \times 8$ | 4.10 | 0.001 | $1.5(1.3) \times 10^{-5}$ | 0.036(11) | 0.0125(50) | 0.975(3) | 0.097(38) | −0.010(5) |
| $32^3 \times 12$ | 4.23 | 0.01 | 0.011(1) | 0.112(10) | 0.109(4) | 0.038(4) | 0.11(1) | 0.064(11) |
| $32^3 \times 12$ | 4.23 | 0.005 | 0.00444 (96) | 0.107(11) | 0.107(8) | 0.083(9) | 0.115(16) | 0.026(7) |
| $32^3 \times 12$ | 4.23 | 0.0025 | 0.0017(4) | 0.186(47) | 0.216(41) | 0.162(22) | 0.162(40) | 0.0065(20) |
| $32^3 \times 12$ | 4.24 | 0.01 | 0.011(1) | 0.135(8) | 0.101(3) | 0.046(3) | 0.107(14) | 0.065(10) |
| $32^3 \times 12$ | 4.24 | 0.005 | 0.0054(9) | 0.112(17) | 0.124(13) | 0.057(10) | 0.122(21) | 0.030(14) |
| $32^3 \times 12$ | 4.24 | 0.0025 | 0.0008(5) | 0.052(15) | 0.041(13) | 0.32(8) | 0.078(52) | 0.0030(6) |

The results for $\Delta^{\text{direct}}_{\pi-\delta}$ and $\Delta^{\text{ev}}_{\pi-\delta}$ are presented in Table III. The saturation of the low-mode approximation is demonstrated in Fig. 11 for two typical configurations.

Next, let us separate the contribution coming from the violation of the Ginsparg-Wilson relation. As we already discussed in [34], $\Delta^{\text{ev}}_{\pi-\delta}$ can be decomposed into the chiral symmetric part $\Delta^{\text{GW}}_{\pi-\delta}$ and violating part $\Delta^{\not{\text{GW}}}_{\pi-\delta}$ as

$$\Delta^{\text{ev}}_{\pi-\delta} = \Delta^{\text{GW}}_{\pi-\delta} + \Delta^{\not{\text{GW}}}_{\pi-\delta}, \tag{20}$$

$$\Delta^{\text{GW}}_{\pi-\delta} \equiv \frac{1}{V(1-m^2)^2}\sum_i \frac{2m^2(1-\lambda_i^{(m)2})^2}{\lambda_i^{(m)4}}, \tag{21}$$

$$\Delta^{\not{\text{GW}}}_{\pi-\delta} \equiv \frac{1}{V(1-m)^2}\sum_i \left[\frac{h_i}{\lambda_i^{(m)}} - 4\frac{g_i}{\lambda_i^{(m)}}\right], \tag{22}$$

where $g_i$ was already defined in Eq. (19) and

$$h_i \equiv \frac{2(1-m)^2}{(1+m)}\psi_i^\dagger\gamma_5(H^{\text{4D}}_{\text{DW}}(m))^{-1}\gamma_5\Delta_{\text{GW}}(H^{\text{4D}}_{\text{DW}}(m))^{-1}\psi_i + \frac{2}{1+m}\left(1+\frac{m}{\lambda_i^{(m)2}}\right)g_i \tag{23}$$

is another measure of the violation of Ginsparg-Wilson relation. Both of these quantities must be zero if the Ginsparg-Wilson relation is satisfied.

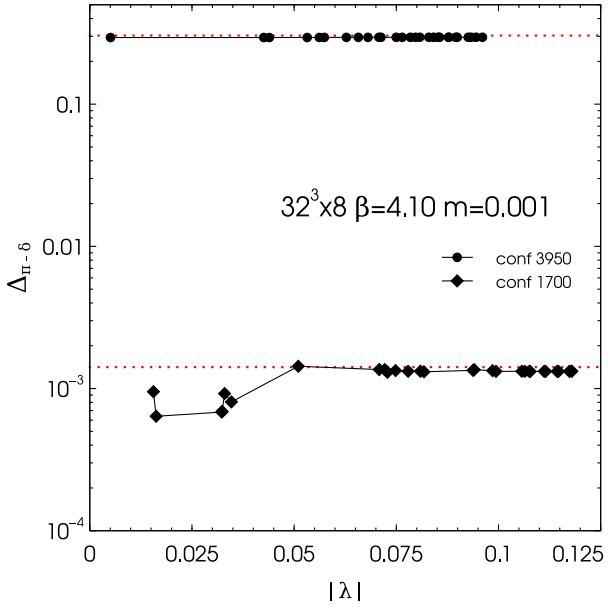


FIG. 11. Low-mode saturation of $\Delta_{\pi-\delta}$. The horizontal axis shows the threshold of the eigenvalue, below which $\Delta^{\text{ev}}_{\pi-\delta}$ is computed. The data for two typical configurations generated with $\beta = 4.10$, $ma = 0.001$ on the $32^3 \times 8$ lattice are shown. The dotted lines are the results for the direct computation $\Delta^{\text{direct}}_{\pi-\delta}$.

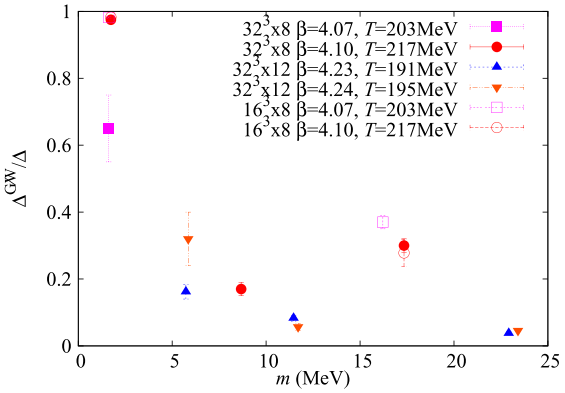


FIG. 12. Quark mass dependence of the ratio $\Delta^{\not{\text{GW}}}_{\pi-\delta}/\Delta_{\pi-\delta}$. The contribution from the chirality violating terms dominates the signal near the chiral limit.

Figure 12 shows the quark mass dependence of the ratio $\Delta^{\not{\text{GW}}}_{\pi-\delta}/\Delta^{\text{ev}}_{\pi-\delta}$. The Ginsparg-Wilson relation violating part $\Delta^{\not{\text{GW}}}_{\pi-\delta}$ dominates the signal as the quark mass decreases. For data points less than $m = 5$ MeV (at lower $\beta$), more than 60%–98% of the signal is the contribution from $\Delta^{\not{\text{GW}}}_{\pi-\delta}$. Thus, we need a careful control of the chiral symmetry on the low-lying eigenmodes in taking the chiral limit of the $U(1)_A$ breaking observables.

Finally, let us examine the $U(1)_A$ susceptibility with overlap fermions. Here we do not use the partially quenched overlap as we have shown its significant lattice artifacts. We observe that the partially quenched overlap $\Delta_{\pi-\delta}$ overshoots the Möbius domain-wall data. We confirm that $g_i$ and $h_i$ for the overlap Dirac eigenmodes are negligible (see Fig. 10), so that we can safely use $\Delta^{\text{GW}}_{\pi-\delta}$ together with the OV/DW reweighting to estimate the $U(1)_A$ susceptibility (let us denote it as $\Delta^{\text{ov}}_{\pi-\delta}$).

Taking the advantage of good chirality, we can subtract the effect of the chiral zero-mode effects [73],

$$\bar{\Delta}^{\text{ov}}_{\pi-\delta} \equiv \Delta^{\text{ov}}_{\pi-\delta} - \frac{2N_0}{Vm^2}. \tag{24}$$

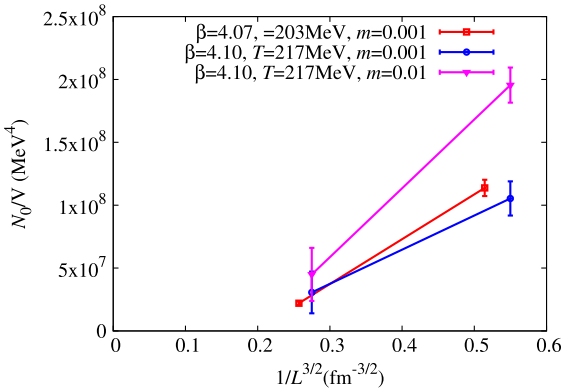


FIG. 13. The lattice size $L$ dependence of $\langle N_0/V\rangle$. The results at $L_t = 8$ are shown.

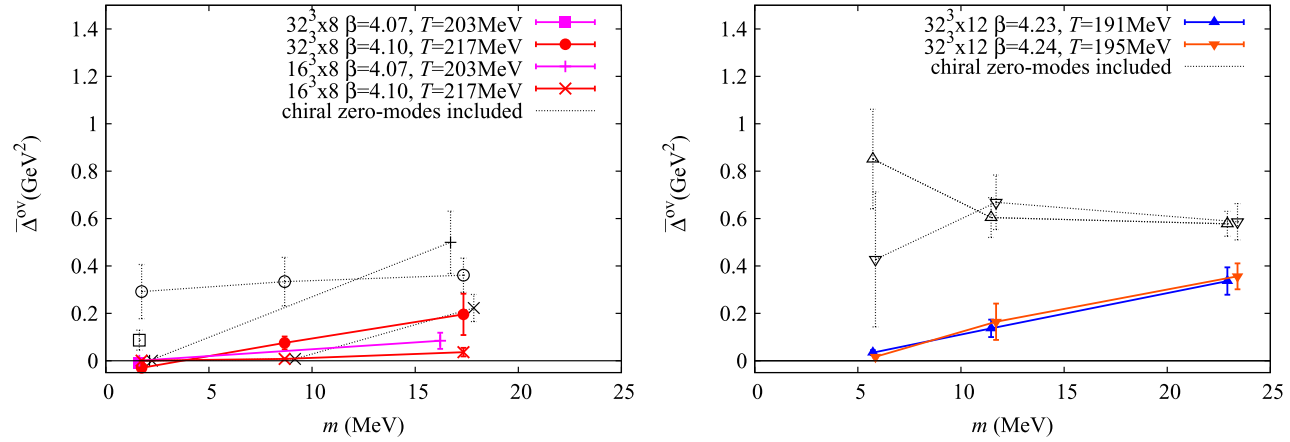


FIG. 14. The quark mass dependence of $\bar{\Delta}^{ov}_{\pi-\delta}$ (solid symbols) and $\Delta^{ov}_{\pi-\delta}$ (dashed). Data for coarse (left panel) and fine (right) lattices are shown.

The expectation value of $N_0^2$ is expected to be an $O(V)$ quantity, as shown in [26], so that these chiral zero-mode's effects should not survive in the large volume limit, as $N_0/V$ is vanishing as $O(1/\sqrt{V})$. We numerically confirm the monotonically decreasing volume scaling of $\langle N_0/V\rangle$ as shown in Fig. 13. Therefore, $\bar{\Delta}^{ov}_{\pi-\delta}$ and $\Delta^{ov}_{\pi-\delta}$ are guaranteed to have the same thermodynamical limit. We also confirm that the 5–15 lowest modes are enough to saturate the reweighing for $\bar{\Delta}^{ov}_{\pi-\delta}$ on $32^3\times 8$ lattices.

Our results for $\bar{\Delta}^{ov}_{\pi-\delta}$ (solid symbols) and $\Delta^{ov}_{\pi-\delta}$ (dashed) are plotted in Fig. 14. We confirm that our data for $\bar{\Delta}^{ov}_{\pi-\delta}$ are stable against the change of the lattice size and lattice spacing, and their chiral limits are all consistent with zero. Precisely, all our data are well described (with $\chi^2/\text{d.o.f}\lesssim 1$) by a simple linear function, which becomes consistent with zero "before" the chiral limit. We list the linear extrapolation of $\bar{\Delta}^{ov}_{\pi-\delta}$ at $m_{ud}=4$ MeV [74] in Table IV. We observe neither strong volume dependence nor $\beta$ dependence of this behavior. Taking the largest value in the table, we conclude that the chiral limit of $\bar{\Delta}^{ov}_{\pi-\delta}$ is estimated to be at most 0.0040(130) GeV$^2$. Although our naive linear extrapolation may simply fail to detect higher order mass dependence, the smallness of $\bar{\Delta}^{ov}_{\pi-\delta}$ itself compared to the data around $m_{ud}=20$ MeV is significative and has a phenomenological importance.

TABLE IV. Linear extrapolation of $\bar{\Delta}^{ov}_{\pi-\delta}$ to $m_{md}=4$ MeV. It becomes consistent with zero before the chiral limit.

| $L^3\times L_t$ | $\beta$ | $T$ (MeV) | $\bar{\Delta}^{ov}_{\pi-\delta}$[GeV$^2$] at $m_{ud}=4$ MeV | $\chi^2$/d.o.f. |
|---|---|---|---|---|
| $32^3\times 12$ | 4.23 | 191(1) | 0.0037(099) | 0.002 |
| $32^3\times 12$ | 4.24 | 195(1) | −0.0199(033) | 0.2 |
| $16^3\times 8$ | 4.10 | 217(1) | 0.0025(017) | 1.0 |
| $32^3\times 8$ | 4.10 | 217(1) | 0.0040(130) | 0.01 |

## V. CONCLUSION

In this work, we have examined the $U(1)_A$ anomaly in two-flavor lattice QCD at a finite temperature with chiral fermions. On the configurations generated by the Möbius domain-wall Dirac quarks, we have measured the Dirac eigenvalue spectrum of both the Möbius domain-wall and overlap quarks, with or without OV/DW reweighting. We have also examined the meson susceptibility difference $\Delta_{\pi-\delta}$, that directly measures the violation of the $U(1)_A$ symmetry. Our ensembles are generated at slightly above the critical temperature of the chiral phase transition ($T\sim 190$–$220$ MeV) on different physical volume sizes ($L=2$–$4$ fm), where frequent topology tunnelings occur.

Our results for the histograms of the Möbius domain wall and (reweighted) overlap Dirac operators both show a strong suppression of the near zero modes as the quark mass decreases. This behavior is stable against the change of the lattice size and lattice spacing.

If we do not perform the reweighting of their determinants, the overlap Dirac spectrum shows unphysical peaks near zero. We have identified them as partially quenched lattice artifacts, due to the strong violation of the Ginsparg-Wilson relation in the low-lying eigenmodes of the Möbius domain-wall operator. Our analysis indicates a potential danger in taking the chiral limit of any observables with domain-wall type fermions even when the residual mass is small. If the observable target is sensitive to the low-lying modes and their chiral properties, its chiral limit can be distorted by the lattice artifacts.

After removal of these artifacts by the OV/DW reweighting procedure, we have found that the $U(1)_A$ susceptibility is consistent with zero in the chiral limit. From these evidences, we conclude that $U(1)_A$ symmetry breaking in two-flavor QCD is consistent with zero above the critical temperature around 200 MeV in the vanishing quark mass limit.

## ACKNOWLEDGMENTS

We thank K. Hashimoto, K. Kanaya, T. Kanazawa, Y. Taniguchi for discussions. We also thank the members of JLQCD Collaboration for their support on this work. Discussions during the YITP workshop YITP-T-14-03 on Hadrons and Hadron Interactions in QCD were helpful to complete this work. AT received generous support from H-T. Ding. Numerical simulations are performed on IBM System Blue Gene Solution at High Energy Accelerator Research Organization (KEK) under a support for is Large Scale Simulation Program (Grant No. 14/15-10). This research was supported by MEXT as a priority issue on the Post-K computer (Elucidation of the Fundamental Laws and Evolution of the Universe). This work is supported in part by JSPS KAKENHI (Grants No. JP25800147, No. JP26247043, No. JP26400259, and No. JP15K05065, JP16H03978), and by MEXT SPIRE and JICFuS. GC is supported by STFC, Grant No. ST/L000458/1. AT is supported by NSFC under Grant No. 11535012.

[1] D. J. Gross, R. D. Pisarski, and L. G. Yaffe, Rev. Mod. Phys. **53**, 43 (1981).
[2] R. D. Pisarski and F. Wilczek, Phys. Rev. D **29**, 338 (1984).
[3] The original argument of [2] was based on the one-loop computation of the effective meson theory. The order of the QCD chiral phase transition is a subject of active studies. The recent developments are found in Refs. [4–17].
[4] G. Cossu, M. D'Elia, A. Di Giacomo, and C. Pica, arXiv:0706.4470.
[5] A. Pelissetto and E. Vicari, Phys. Rev. D **88**, 105018 (2013).
[6] K. I. Ishikawa, Y. Iwasaki, Y. Nakayama, and T. Yoshie, Phys. Rev. D **89**, 114503 (2014).
[7] Y. Nakayama and T. Ohtsuki, Phys. Rev. D **91**, 021901 (2015).
[8] G. Fejos, Phys. Rev. D **90**, 096011 (2014).
[9] M. Grahl, Phys. Rev. D **90**, 117904 (2014).
[10] T. Kanazawa and N. Yamamoto, Phys. Rev. D **91**, 105015 (2015).
[11] T. Sato and N. Yamada, Phys. Rev. D **91**, 034025 (2015).
[12] E. Meggiolaro, Nucl. Part. Phys. Proc. **273–275**, 1502 (2016).
[13] T. Kanazawa and N. Yamamoto, J. High Energy Phys. 01 (2016) 141.
[14] J. Eser, M. Grahl, and D. H. Rischke, Phys. Rev. D **92**, 096008 (2015).
[15] S. Ejiri, R. Iwami, and N. Yamada, Phys. Rev. D **93**, 054506 (2016).
[16] Y. Nakayama and T. Ohtsuki, Phys. Rev. Lett. **117**, 131601 (2016).
[17] C. Bonati, P. de Forcrand, M. D'Elia, O. Philipsen, and F. Sanfilippo, Phys. Rev. D **90**, 074030 (2014).
[18] E. Berkowitz, M. I. Buchoff, and E. Rinaldi, Phys. Rev. D **92**, 034507 (2015).
[19] R. Kitano and N. Yamada, J. High Energy Phys. 10 (215) 136.
[20] P. Petreczky, H.-P. Schadler, and S. Sharma, Phys. Lett. B **762**, 498 (2016).
[21] S. Borsanyi *et al.*, Nature (London) **539**, 69 (2016).
[22] C. Bonati, M. D'Elia, M. Mariti, G. Martinelli, M. Mesiti, F. Negro, F. Sanfilippo, and G. Villadoro, J. High Energy Phys. 03 (2016) 155.
[23] T. D. Cohen, Phys. Rev. D **54**, R1867 (1996).
[24] T. D. Cohen, arXiv:nucl-th/9801061.
[25] M. C. Birse, T. D. Cohen, and J. A. McGovern, Phys. Lett. B **388**, 137 (1996).
[26] S. Aoki, H. Fukaya, and Y. Taniguchi, Phys. Rev. D **86**, 114512 (2012).
[27] G. Cossu, S. Aoki, H. Fukaya, S. Hashimoto, T. Kaneko, H. Matsufuru, and J.-I. Noaki, Phys. Rev. D **87**, 114514 (2013).
[28] T.-W. Chiu, W.-P. Chen, Y.-C. Chen, H.-Y. Chou, and T.-H. Hsieh (TWQCD Collaboration), *Proc. Sci.*, LATTICE2013 (2014) 165.
[29] B. B. Brandt, A. Francis, H. B. Meyer, O. Philipsen, D. Robaina, and H. Wittig, J. High Energy Phys. 12 (2016) 158.
[30] V. Azcoiti, Phys. Rev. D **94**, 094505 (2016).
[31] A. Bazavov *et al.* (HotQCD Collaboration), Phys. Rev. D **86**, 094503 (2012).
[32] M. I. Buchoff, M. Cheng, N. H. Christ, H. T. Ding, C. Jung *et al.*, Phys. Rev. D **89**, 054514 (2014).
[33] V. Dick, F. Karsch, E. Laermann, S. Mukherjee, and S. Sharma, Phys. Rev. D **91**, 094504 (2015).
[34] G. Cossu, H. Fukaya, S. Hashimoto, and A. Tomiya (JLQCD Collaboration), Phys. Rev. D **93**, 034507 (2016).
[35] P. H. Ginsparg and K. G. Wilson, Phys. Rev. D **25**, 2649 (1982).
[36] We do not observe such a large violation of chirality at low temperature. It seems that this problem arises only at $T > T_c$. One can intuitively understand the qualitative difference between $T > T_c$ and $T < T_c$ by the amount of the physical near-zero modes, which survive in the continuum limit. At $T < T_c$, there are dense physical modes mixing with the lattice artifact and make the effect of the violation of chiral symmetry relatively small, while at $T > T_c$, the unphysical near zero may give a dominant effect on the low-energy observables.
[37] R. Brower, H. Neff, and K. Orginos, Nucl. Phys. B, Proc. Suppl. **153**, 191 (2006).
[38] R. C. Brower, H. Neff, and K. Orginos, arXiv:1206.5214.
[39] H. Neuberger, Phys. Lett. B **417**, 141 (1998).
[40] H. Neuberger, Phys. Rev. Lett. **81**, 4060 (1998).
[41] M. Luscher, Physica B (Amsterdam) **428**, 342 (1998).
[42] H. Fukaya, S. Hashimoto, K.-I. Ishikawa, T. Kaneko, H. Matsufuru, T. Onogi, and N. Yamada (JLQCD Collaboration), Phys. Rev. D **74**, 094505 (2006).

[43] S. Aoki *et al.* (JLQCD Collaboration), Phys. Rev. D **78**, 014508 (2008).
[44] S. Sharma, V. Dick, F. Karsch, E. Laermann, and S. Mukherjee, Nucl. Phys. **A956**, 793 (2016).
[45] G. Cossu, H. Fukaya, S. Hashimoto, T. Kaneko, J.-i. Noaki, and A. Tomiya (JLQCD), *Proc. Sci.*, LATTICE2014 (2015) 210.
[46] A. Tomiya, G. Cossu, H. Fukaya, S. Hashimoto, and J. Noaki, *Proc. Sci.*, LATTICE2014 (2015) 211.
[47] G. Cossu, H. Fukaya, S. Hashimoto, J.-i. Noaki, and A. Tomiya (JLQCD Collaboration), *Proc. Sci.*, LATTICE2015 (2016) 196.
[48] S. Aoki (JLQCD Collaboration), *Proc. Sci.*, CD15 (2016) 045.
[49] Y. Shamir, Nucl. Phys. **B406**, 90 (1993).
[50] V. Furman and Y. Shamir, Nucl. Phys. **B439**, 54 (1995).
[51] D. B. Kaplan, Phys. Lett. B **288**, 342 (1992).
[52] S. Hashimoto, S. Aoki, G. Cossu, H. Fukaya, T. Kaneko *et al.*, *Proc. Sci.*, LATTICE2013 (2014) 431.
[53] M. Luscher and P. Weisz, Phys. Lett. **158B**, 250 (1985).
[54] C. Morningstar and M. J. Peardon, Phys. Rev. D **69**, 054501 (2004).
[55] G. Cossu, J. Noaki, S. Hashimoto, T. Kaneko, H. Fukaya, P. A. Boyle, and J. Doi, arXiv:1311.0084.
[56] T. Kaneko, S. Aoki, G. Cossu, H. Fukaya, S. Hashimoto, and J. Noaki (JLQCD Collaboration), *Proc. Sci.*, LATTICE2013 (2014) 125.
[57] R. Sommer, *Proc. Sci.*, LATTICE2013 (2014) 015.
[58] R. G. Edwards, U. M. Heller, and T. R. Klassen, Nucl. Phys. **B517**, 377 (1998).
[59] S. A. Larin and J. A. M. Vermaseren, Physica B (Amsterdam) **303**, 334 (1993).
[60] W. E. Caswell, Phys. Rev. Lett. **33**, 244 (1974).
[61] D. R. T. Jones, Nucl. Phys. **B75**, 531 (1974).
[62] E. Egorian and O. V. Tarasov, Teor. Mat. Fiz. **41**, 26 (1979) [Theor. Math. Phys. **41**, 863 (1979)].
[63] M. Luscher, J. High Energy Phys. 08 (2010) 071; 03 (2014) 92(E).
[64] In our typical simulations, $H_{\rm ov}(m)$ eigenvalues/eigenvectors computation for one configuration costs roughly the same as 10–30 trajectories of the HMC run. That for $H_M$ is 10 times faster. However, these numerical costs strongly depend on temperature and how many eigenvalues we need.
[65] H. Fukaya *et al.* (JLQCD Collaboration), *Proc. Sci.*, LATTICE2013 (2014) 127.
[66] A. Hasenfratz, R. Hoffmann, and S. Schaefer, Phys. Rev. D **78**, 014515 (2008).
[67] K. Ogawa and S. Hashimoto, Prog. Theor. Phys. **114**, 609 (2005).
[68] For our recent study of the chiral symmetry breaking at zero temperature, see Ref. [69].
[69] G. Cossu, H. Fukaya, S. Hashimoto, T. Kaneko, and J.-I. Noaki, Prog. Theor. Exp. Phys. **2016**, 093B06 (2016).
[70] The detailed study of the individual eigenmodes and their localization properties is also reported in Ref. [71].
[71] G. Cossu and S. Hashimoto, J. High Energy Phys. 06 (2016) 056.
[72] We thank Y. Shamir for the suggestion for the improvement by subtracting $m_{\rm res}$.
[73] The eigenmode decomposition is given in Eq. (3.11) of our previous work [34], from which we can identify the zero-mode contribution is $2N_0/Vm^2$.
[74] Because we do not renormalize the quark mass, our data do not represent physically equal mass points. However, their difference is expected to be smaller than the statistical errors and systematic errors of the fit. The conclusion does not change if we choose $m_{\rm ud} < 5$ MeV.